ADVANCES IN ATMOSPHERIC SCIENCES, VOL. 34, SEPTEMBER 2017, 1106–1120

• **Original Paper** •

The Role of Initial Cloud Condensation Nuclei Concentration in Hail Using the WRF NSSL 2-moment Microphysics Scheme

Xiaofei LI, Qinghong ZHANG*, and Huiwen XUE

Department of Atmospheric and Oceanic Sciences, School of Physics, Peking University, Beijing 100871*, China*

(Received 8 September 2016; revised 30 March 2017; accepted 10 April 2017)

ABSTRACT

The effects of the initial cloud condensation nuclei (CCN) concentrations (100–3000 mg^{-1}) on hail properties were investigated in an idealized non-severe hail storm experiment using the Weather Research and Forecasting (WRF) model, with the National Severe Storms Laboratory 2-moment microphysics scheme. The initial CCN concentration (CCNC) had obvious non-monotonic effects on the mixing ratio, number concentrations, and radius of hail, both in clouds and at the surface, with a CCNC threshold between 300 and 500 mg^{-1}. An increasing CCNC is conducive (suppressive) to the amount of surface hail precipitation below (above) the CCNC threshold. The non-monotonic effects were due to both the thermodynamics and microphysics. Below the CCNC threshold, the mixing ratios of cloud droplets and ice crystals increased dramatically with the increasing CCNC, resulting in more latent heat released from condensation and frozen between 4 and 8 km and intensified updraft volume. The extent of the riming process, which is the primary process for hail production, increased dramatically. Above the CCNC threshold, the mixing ratio of cloud droplets and ice crystals increased continuously, but the maximum updraft volume was weakened because of reduced frozen latent heating at low level. The smaller ice crystals reduced the formation of hail and smaller clouds, with decreased rain water reducing riming efficiency so that graupel and hail also decreased with increasing CCNC, which is unfavorable for hail growth.

Key words: CCN, hail, microphysics, thermodynamics, threshold

Citation: Li, X. F., Q. H. Zhang, and H. W. Xue, 2017: The role of initial cloud condensation nuclei concentration in hail using the WRF NSSL 2-moment microphysics scheme. *Adv. Atmos. Sci.*, **34**(9), 1106–1120, doi: 10.1007/s00376-017-6237-9.

1. Introduction

Atmospheric aerosol particles have a significant impact on the temporal and spatial development of deep convective storms, some of which can serve as cloud condensation nuclei (CCN) and ice nuclei (IN) in the formation of cloud droplets and ice crystals (Sun and Ariya, 2006). More CCN in a given sounding environment generally result in reduced cloud particle size and suppressed precipitation, such that it may affect the amount and type of precipitation (rain or hail) and thus affect the development of convective cloud (Rosenfeld, 2000; Yin et al., 2000; Rosenfeld et al., 2008; Andreae and Rosenfeld, 2008; Noppel et al., 2010; Mansell and Ziegler, 2013; Guo et al., 2015). China is suffering from worsening air pollution; long-lasting episodes of severe haze have occurred in recent years. The mean value of the CCN concentration (CCNC) at the surface has been reported to be over 2500 cm^{-3} in haze conditions during spring and autumn in central and northern China (Sun et al., 2012; Jia et al., 2016). Consequently, it is important to determine whether hail will be influenced by the anthropogenic air pollution that is creating higher CCN in China. The monsoon area covers approximately 60% of mainland China in summer (Jiang et al., 2015), and soundings in the China monsoon area are different from those used in previous studies (Mansell and Ziegler, 2013; Carrió et al., 2014; Loftus and Cotton, 2014). The maximum hail diameter of around 5–10 mm is the most common maximum hail size in the Inner Mongolia Autonomous Region in northern China (Xie et al., 2010), where a typical hail storm sounding is weaker than it is in the United States (Mansell and Ziegler, 2013). There was a significant decreasing trend in hail-day frequency from 1961 to 2010, correlating strongly with the weakening of the East Asian summer monsoon (Zhang et al., 2017). The long-term trend of hail-day frequency in China may be affected by aerosols, and this is not fully understood (Li et al., 2016). Little research has been conducted with regard to the CCN effects on hail using idealized simulations in this monsoon region of China in summer, although the typical hail environment is usually weaker than severe hailstorms.

CCN could potentially influence the thermodynamics of the clouds in deep convection, such as cloud top heights, radar reflectivity, and updraft velocity (Khain et al., 2005;

* Corresponding author: Qinghong ZHANG
Email: qzhang@pku.edu.cn

Tao et al., 2007; van den Heever et al., 2011). Microphysical effects are also influenced dramatically by CCN in deep convective clouds. For example, CCN have a substantial influence on the microphysical properties of water and ice clouds, which in turn affect the processes that lead to the formation of hail (Andreae and Rosenfeld, 2008; Rosenfeld et al., 2008; Liu and Niu, 2010; Fan et al., 2013). Some previous numerical simulations have indicated that an increased CCNC slows warm-rain processes, so that more cloud water is carried up to the freezing level and more latent heat is released to reinforce the updraft. More supercooled water is then potentially available for riming by frozen particles (van den Heever et al., 2006; Khain et al., 2011; Carrió et al., 2014; Loftus and Cotton, 2014). Several numerical studies have attempted to simulate CCN effects on cloud microphysics and dynamics (Xiao et al., 1988; Seifert et al., 2006; Noppel et al., 2010; Khain et al., 2011; Yang et al., 2011; Carrió et al., 2014; Loftus and Cotton, 2014).

A variety of numerical simulations have demonstrated the monotonic effect of CCN on hail (Noppel et al., 2010; Khain et al., 2011; Yang et al., 2011). Noppel et al. (2010) performed a study combining four different CCN assumptions, from 100 cm^{-3} to 2100 cm^{-3}, with a broad cloud droplet size distribution, using a simple two-moment bulk scheme, and found that hail precipitation decreased with increasing CCNC for a midlatitude storm in the southwest of Germany. However, Khain et al. (2011) simulated the same hail storm with a two-dimensional (2D) bin scheme, with the opposite result, showing that an increase in CCNC from 100 to 3000 cm^{-3} led to an increase in accumulated rain, with the hail mass and the mass of supercooled water determining the efficiency of riming and formation of large graupel and hail. These conflicting results could be due to differences in the microphysics scheme and the model configuration. It is suggested that different model setups and more sophisticated microphysics should be used in future studies (Grabowski, 2014, 2015). As CCNC increased from 300 to 5000 cm^{-3} in Hebei Province, China, in a real-case run, the mixing ratios of small cloud droplets and large ice-phase hydrometeor particles including aggregates and graupel increased, while the mixing ratios of large cloud droplets and rain drops and of small ice-phase particles including pristine ice and snow decreased. The hail number concentration and mixing ratio tended to decrease, but the mean diameter of hail increased with large CCNC in a two-moment bulk approach (Yang et al., 2011).

However, other independent studies found a nonmonotonic response of hail to CCN (Carrió et al., 2014; Loftus and Cotton, 2014). Carrió et al. (2014) found that a peak of simulated hail number concentration at the surface for CCNC between 1500 and 2000 cm^{-3} occurred for high cloud-base heights in the United States in a triple-moment approach. However, the influence of CCN on hail-increasing processes and hail-decreasing processes were not addressed from a microphysics perspective. A similar nonmonotonic response of maximum precipitation rates and hail number concentration was found at the surface. Another triple-moment bulk microphysics scheme, with a sounding near Goodland in the United States, showed that increases in potential CCNC led to non-monotonic responses in nearly all hydrometeor fields, and the overall storm dynamics and evolution were largely unaffected, whereas storms with higher CCNC did not produce hail at the surface in a two-moment approach (Loftus and Cotton, 2014). The detailed conducive or suppressive effects of CCN on hail remain largely unknown from the perspective of microphysics combined with dynamics.

There are several widely used microphysical parameterization models for in-cloud processes, including Lagrangian trajectory, bin, bulk, and hybrid bin parameterization models (Straka, 2009). Both the complete two-moment bulk microphysical scheme and the spectral bin model have predicted similar evolution of the important microphysical and dynamical variables (Seifert et al., 2006). In the present study, the relatively complicated National Severe Storm Laboratory (NSSL) 2-moment scheme in the Weather Research and Forecasting (WRF) model was used to consider the effects of different initial CCNC on hail from an idealized hail storm with a non-severe but typical hail case sounding in the monsoon area, based on a real case in China. Although the IN effect is important in microphysics processes, this study focused only on CCN effects on hail. Even though the NSSL 2-moment scheme cannot represent multimodal distributions, it has an additional option to predict the CCNC, which is intended for idealized cloud-resolving simulations. Further effort was made to investigate the effects of CCN on the characteristics of hail and other hydrometeor particles (cloud droplets, rain droplets, ice crystals, snow, and graupel), both in clouds and at the surface. A brief description of the microphysics scheme and the simulation design of the sensitivity experiments are given in section 2. Results are presented in section 3, followed by conclusions in section 4.

2. Microphysics scheme and experimental design

2.1. *NSSL 2-moment microphysics*

The Advanced Research WRF (WRF-ARW) model, version 3.7.1 (NCAR, 2015) was used in this study. The model is fully compressible and non-hydrostatic, with a run-time hydrostatic option. The NSSL 2-moment scheme (Ziegler, 1985; Mansell et al., 2010; Mansell et al., 2010; Mansell and Ziegler, 2013) is a bulk scheme that predicts the mass mixing ratio and number concentrations of all hydrometeor species (cloud droplets, rain drops, ice crystals, snow, graupel, and hail). It also predicts average graupel particle density, and allows graupel to span the range from frozen drops to low-density graupel. There is an additional option in WRF-ARW to predict the CCNC (intended for idealized simulations). The scheme is intended for cloud-resolving simulations in research applications (Wang et al., 2016b).

The initiation of cloud droplets follows Mansell et al. (2010). The rates of cloud droplet number concentration R_c initiated at the cloud base is calculated as

$$R_c = \frac{1}{\Delta t} 10^6 (10^{-6} C_{CCN})^{\frac{2}{k+2}} \left[\frac{1.63 w^{\frac{3}{2}}}{kB\left(\frac{3}{2}, \frac{k}{2}\right)} \right]^{\frac{k}{k+2}}, \quad (1)$$

where C_{CCN} is the assumed CCNC at the specific height, k is the exponent, w is the updraft speed, Δt is the time step, and B is the complete beta function.

The default primary ice nucleation rate R_I in this scheme is parameterized as Eq. (2) and Eq. (3) given by Phillips et al. (2008), where A_1 is 12.96, A_2 is 0.639, S_i is the saturation ratio of water vapor with respect to ice, T is Kelvin temperature, and C_{IN} is the default IN number concentration, which is 1000 kg^{-1}:

$$R_I = 0.06 C_{IN} e^{\min(57.0, [A_1(S_i - 1) - A_2])} \quad (243.15 < T < 268.15), \quad (2)$$

$$R_I = 1000 (e^{\min(57.0, A_1(S_i - 1))})^{0.03} \quad (T \leqslant 243.15). \quad (3)$$

Both hail and graupel densities can be predicted in this scheme, for which the allowed ranges are 500–900 kg m^{-3} and 300–900 kg m^{-3}. Graupel fall speeds follow the function given by Mansell (2010), with the drag coefficient ranging from 0.45 to 0.8. Hail fall speed is treated the same as that of graupel, except that the drag coefficient ranges from 0.45 to 0.6. The hail-growth process contains the following processes: deposition of vapor to hail, collection of cloud droplets by hail, collection of rain water by hail, collection of ice crystals by hail, collection of snow by hail, and conversion of graupel to hail. The hail-reducing process contains the following processes: sublimation of hail, shedding of hail to rain, melting of hail to rain, and multiplication of ice (Cotton et al., 1986). The total hail distribution is subdivided by the threshold diameter D_{wet} into two parts that are represented by dry and wet growth. The conversion of graupel to hail is assumed to occur when wet growth conditions exist. Furthermore, the conversion is only allowed at temperatures below −2°C to avoid spurious conversion too close to the melting level.

Collection rate of rain water by hail is a two-component process that take the following forms for the collection of mixing ratio and number concentration, where h refers to hail and r refers to rain drops:

$$\Delta V_{h,r} = [(V_h - V_r)^2 + 0.04 V_h V_r]^{\frac{1}{2}}; \quad (4)$$

$$q_{hacr} = \frac{\pi}{4} E_{h,r} n_h q_r \Delta V_{h,r} (\delta_h^0 \overline{D}_h^2 + \delta_{h,r}^1 \overline{D}_h \overline{D}_r + \delta_r^1 \overline{D}_r^2); \quad (5)$$

$$n_{hacr} = \frac{\pi}{4} E_{h,r} n_h n_r \Delta V_{h,r} (\delta_h^0 \overline{D}_h^2 + \delta_{h,r}^0 \overline{D}_h \overline{D}_r + \delta_r^0 \overline{D}_r^2). \quad (6)$$

Here, V is the mean fall speed, $\Delta V_{h,r}$ is the mean fall speed difference between hail rain drops, q_{hacr} is the collection rate of mixing ratio, n_{hacr} is the collection rate of number concentration, δ is a coefficient function of the shape and exponent, $\overline{D}$ is the mean volume diameter, and E is the average collection efficiency.

Further details of the microphysical scheme can be found in Mansell et al. (2010) and Ziegler (1985).

2.2. *Design of the simulations*

The 3D idealized thunderstorm, which is a preset option in the WRF model, version 3.7.1, was employed to investigate the CCN effects by changing the initial value of the CCNC from 100 to 3000 mg^{-1} (Table 1) at the surface, so that the effects of CCN on thermodynamics and microphysics could be qualified in the absence of other effects including land-surface processes, boundary-layer processes and radiative processes. To make it a well-mixed boundary layer, the CCNC (in units of mg^{-1}) was set to a constant below 2 km and decreasing exponentially from the 2 km height, following Eq. (7):

$$C_{CCN} = C_0 e^{(\frac{H}{H_0})}, \quad (7)$$

where C_0 is the assumed initial CCNC at the surface in Table 1, H is the height above 2 km, and H_0 is 1448 constantly (Duan et al., 2012).

The nested model configuration and convective initialization for the simulations are given in Table 2. The initial thermodynamic conditions for the simulations were given by a Skew-T profile of temperature and dew-point temperature, as shown in Fig. 1. Because of the unsuitable real-station sounding at 0000 UTC for this afternoon-case at 0700 UTC, the profile was based on a real-time high-resolution WRF simulation (1-km resolution in the horizontal direction and 28 levels in the vertical direction, using the NSSL microphysics scheme, but not shown here), using simulated sounding data obtained near Ordos City in China at 0600 UTC 30 June

Table 1. Simulations performed to determine the sensitivity of hail to CCNC.

Simulation	Initial CCN (mg^{-1})
CCN100	100
CCN300	300
CCN500	500
CCN700	700
CCN1000	1000
CCN3000	3000

Table 2. Settings for the nested simulations used in this work.

Model option	Domain 1	Domain 2
Grid	$dx = dy = 1.5$ km	$dx = dy = 500$ m
	260×240 points	355×310 points
Vertical levels	51	51
Model top	20 km	20 km
Time steps	9 s	3 s
Simulation duration	2.5 h	2.5 h
Radiation parameterization	Off	Off
Surface parameterization	Off	Off
Coriolis parameter	9.3×10^{-5} s^{-1}	9.3×10^{-5} s^{-1}
pert_coriolis	On	On

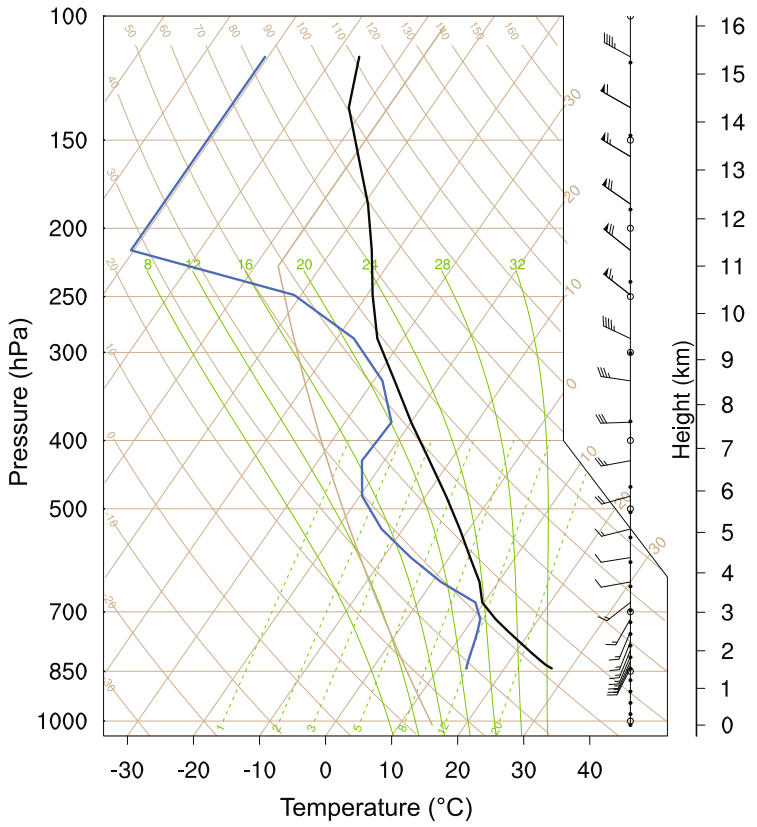

Fig. 1. Skew-T plots of the WRF real-time simulation sounding at 0600 UTC 29 June 2013, near Ordos, China. Black line is the temperature and blue line is the dew point temperature. Brown lines are isotherms (leaned to the right) and the potential temperature (leaned to the left), and solid green lines are the equivalent potential temperature; these three all use the temperature scale at the horizontal 1000 hPa level near the bottom. The scale on the left side is the isobars and the dashed green lines are the saturated humidity mixing ratio. The two scales on the right side are wind-barbs and height scale.

2013. The values of the lifting condensation level, temperature at the lifting condensation level, Showalter index, total precipitable water, and surface-based convective available potential energy (CAPE) were 701 hPa, 11°C, −2, 3 cm, and 1789 J kg^{-1}, respectively. The maximum hailstone diameter was 6 mm, observed at 53543 meteorological observational station in Ordos City on this date, which was the non-severe but typical maximum hail diameter of around 5–10 mm in the Inner Mongolia Autonomous Region in China. It took about 2 h for the evolution of this hail storm, which was located in the central warm area of a trough of low pressure. The forward-tilting trough, the shear line at the low levels and the convergence at the surface provided a favorable circulation background for this hail storm according to the synoptic chart.

3. Results of the simulations

Six simulations were conducted to investigate the impacts of the initial CCNC on hail and other hydrometeors, both in clouds and at the surface. This study focused not only on the thermodynamic but also on the microphysical perspective.

3.1. *Surface hail and total precipitation rate*

Figure 2 shows a time series of the domain-averaged surface hail and total precipitation rates for the cases in Table 1. It was clear that the initial CCNC could potentially modify the behavior of the surface precipitation. There were clear delays in the onset of precipitation with increasing CCNC for this idealized hail storm, in contrast to a previous study that found surface precipitation began at almost the same time for a supercell storm (Loftus and Cotton, 2014). However, the delays consistently matched another previous study's observation that an increase in the initial concentration of CCN led to the formation of a large number of small droplets, with a low collision–coalescence rate, resulting in a time delay in raindrop formation (Khain et al., 2005). The assumption that fewer CCN lead to a faster formation of surface precipitation concurs with the assertion that clouds with low CCNC rain out too quickly to mature into long-lived clouds (Rosenfeld et al., 2008). As the CCNC increased, the maximum hail precipitation rate and accumulated hail precipitation increased

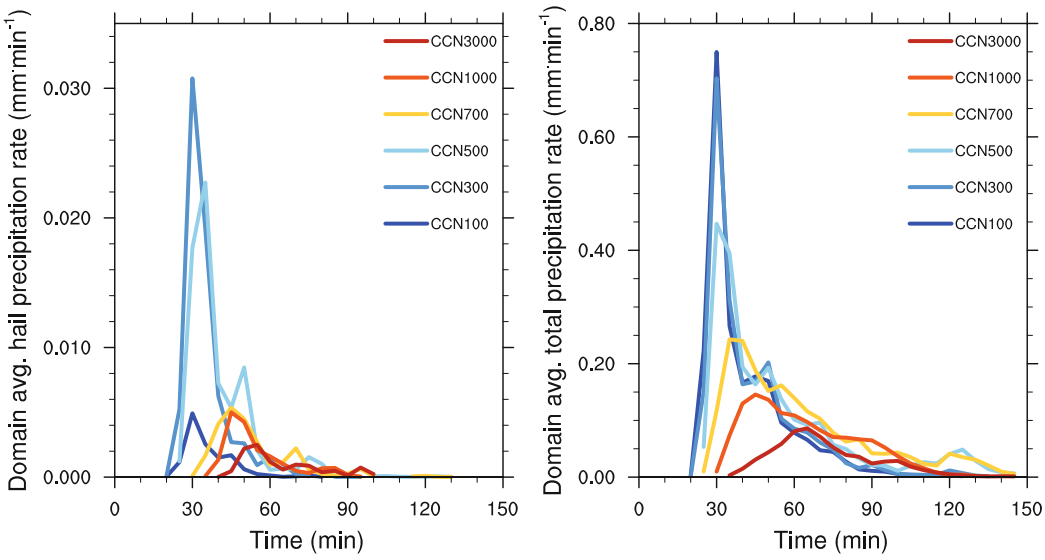

Fig. 2. Time series of domain-averaged surface hail precipitation rate (left) and precipitation rate (right), in mm min^{-1}, for the cases in Table 1.

from cases CCN100 to CCN300, and then decreased when the CCNC was over 500 mg^{-1}. There appeared to be a threshold value at a CCNC between 300 and 500 mg^{-1}, which divided the conducive and suppressive effects of CCNC on the maximum hail precipitation rate and accumulated hail precipitation. The maximum total precipitation rate decreased continuously with increasing CCNC from cases CCN100 to CCN3000. This concurs with the assertion that precipitation is considerably reduced and completely suppressed under highly polluted conditions (Li et al., 2008). These different behaviors of total precipitation and hail precipitation indicate the different effects of CCN on raindrop characteristics and hail characteristics.

3.2. *Effect of CCN concentration on hail characteristics*

The evolution of the domain-averaged mixing ratio and the number concentration of hail in cases CCN100 to CCN3000 (Table 1) at different altitudes are presented in Fig. 3. The hail formed in 20–50 min of simulations in clouds and was delayed slightly from cases CCN100 to CCN3000. The mature stage of hail was also delayed when the initial CCNC was increased in simulations. In cases CCN300 and CCN500, the maximum mixing ratio and number concentration of hail were larger than in the other four cases. The extension of the average hail mixing ratio (exceeding 0.05 mg kg^{-1}) in the vertical orientation increased dramatically to over 10 km when the initial CCNC was increased from cases CCN100 to CCN500. However, the extension of hail in the vertical orientation decreased slightly to 8.5 km as the initial CCNC increased from cases CCN700 to CCN3000.

Figure 4 shows the maximum mixing ratio, maximum number concentration, and maximum mean radius of hail size distribution both in cloud and at the surface for an initial CCNC of 100 to 3000 mg^{-1}. There was a remarkable non-monotonic response of the maximum mixing ratio, number concentration, and radius of hail to the initial CCNC. In the clouds, the maximum mixing ratio, number concentration, and radius of hail increased when the initial CCNC was within the range of 100 to 500 mg^{-1}. All these parameters then decreased after reaching their peak values. At the surface, the values of all these parameters increased at an initial CCNC within a range of 100 to 500 mg^{-1} and then decreased at higher CCNCs. The maximum mean radius of hail was larger than 5.0 mm in cases CCN300 and CCN500, although they were non-severe hailstones. The above analysis indicated that the threshold value of the CCNC between 300 and 500 mg^{-1} was the same for the maximum mixing ratio, number concentration, and radius of hail, both in clouds and at the surface. It would therefore be interesting to investigate whether hail formation and growth depend on the dynamics of the storm and whether the characteristics of all hydrometeors varied with the changes in CCNC (Mansell and Ziegler, 2013).

3.3. *Effect of CCN on thermodynamics*

The simulated maximum reflectivity, updraft volume and microphysics latent heating all showed regular variations in their evolutions with different initial CCNCs. An increase in the CCNC led to a delay in the appearance of the maximum radar composite reflectivity factor from 30 to 60 min, and an extension in the area of radar reflectivity (Fig. 5). The area of increased radar reflectivity (exceeding 20 dBZ) was mainly in the anvil area of the storms, which was due to the large amount of smaller-sized cloud ice particles, leading to greater expansion and much slower dissipation of anvil clouds (Fan et al., 2013). In all six cases, the maximum radar composite reflectivity factor exceeded 50 dBZ. When the CCNC was below the CCNC threshold (cases CCN100 to CCN300), the maximum radar composite reflectivity factor increased from 58 to 59 dBZ; however, it decreased to 50 dBZ

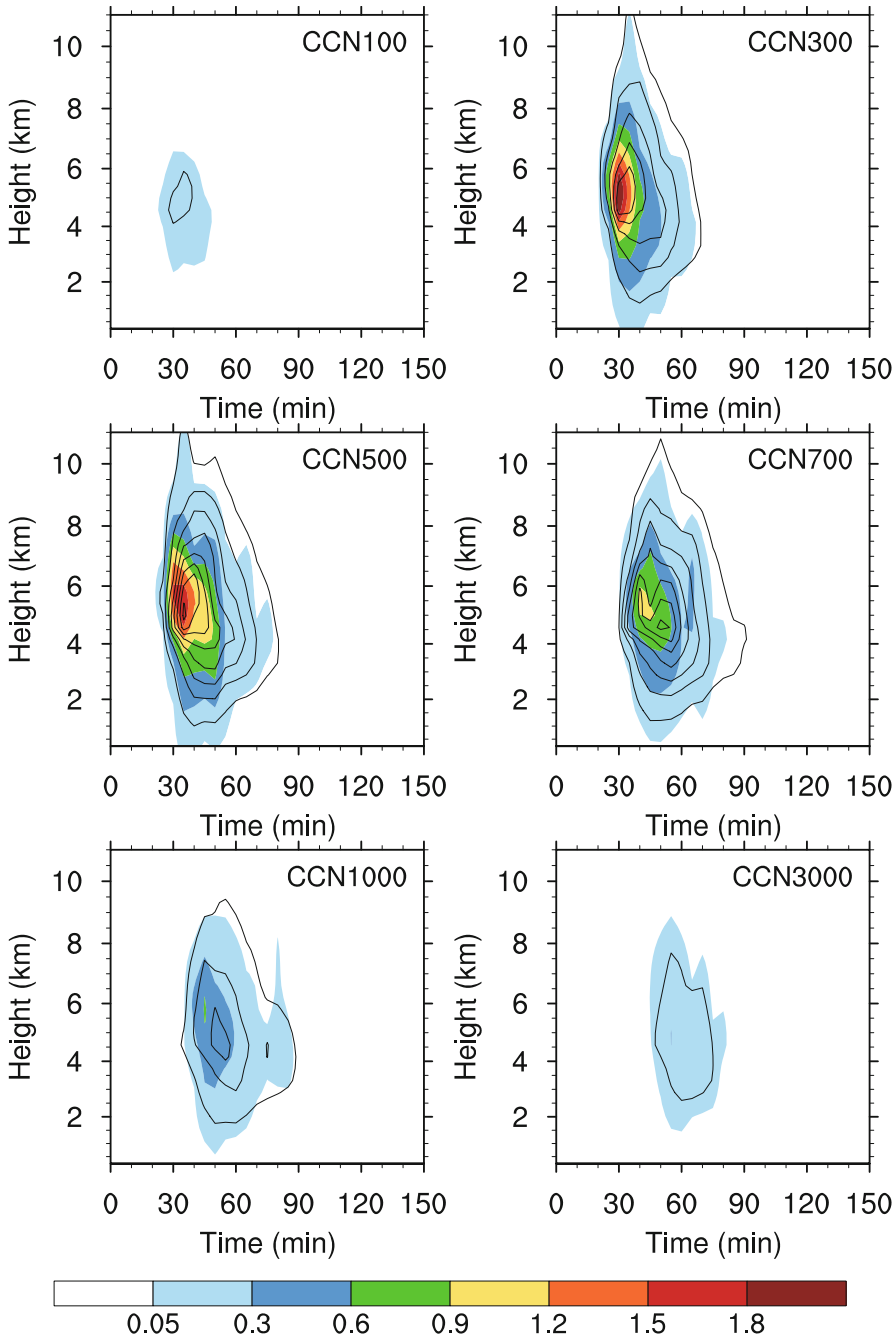

Fig. 3. Time–height contours of domain-averaged hail mixing ratio, in mg kg^{-1}, and hail number concentration, in 10^{-3} kg^{-1} (black contours from 5 to 75 by 10), for the cases in Table 1.

(cases CCN300 to CCN1000) when the CCNC was above the CCNC threshold. The maximum radar composite reflectivity factor is a measurable variable that represents the intensity of a storm or convective intensity (Szoke and Zipser, 1986; Jiang, 2012). Overall, it can be inferred that there was also a CCNC threshold effect on the hail storm intensity, which can be measured by updraft volume (Deierling and Petersen, 2008; Mansell and Ziegler, 2013).

Results showed that the time series of updraft volume (at temperatures colder than −5°C, vertical velocities greater than 10 m s^{-1}, and maximum reflectivity greater than 35 dBZ) had clear relationships with varied CCN (Fig. 6a). The peaks of maximum updraft volume continuously intensified with an increase in the initial CCNC below the CCNC threshold, whereas they weakened above the CCNC threshold. The peaks of the maximum updraft volume increased from 12.3 to 18.0 in 10^{10} m^3, then decreased to 2.9 in 10^{10} m^3, and were evidently affected by the CCNC (Fig. 6a), contrary to previous studies that reported no sensitive aerosol effect on vertical velocity (Khain et al., 2011; Loftus and Cotton, 2014). The discrepancy might be explained by differences in initial sounding, model configuration and storm evolution.

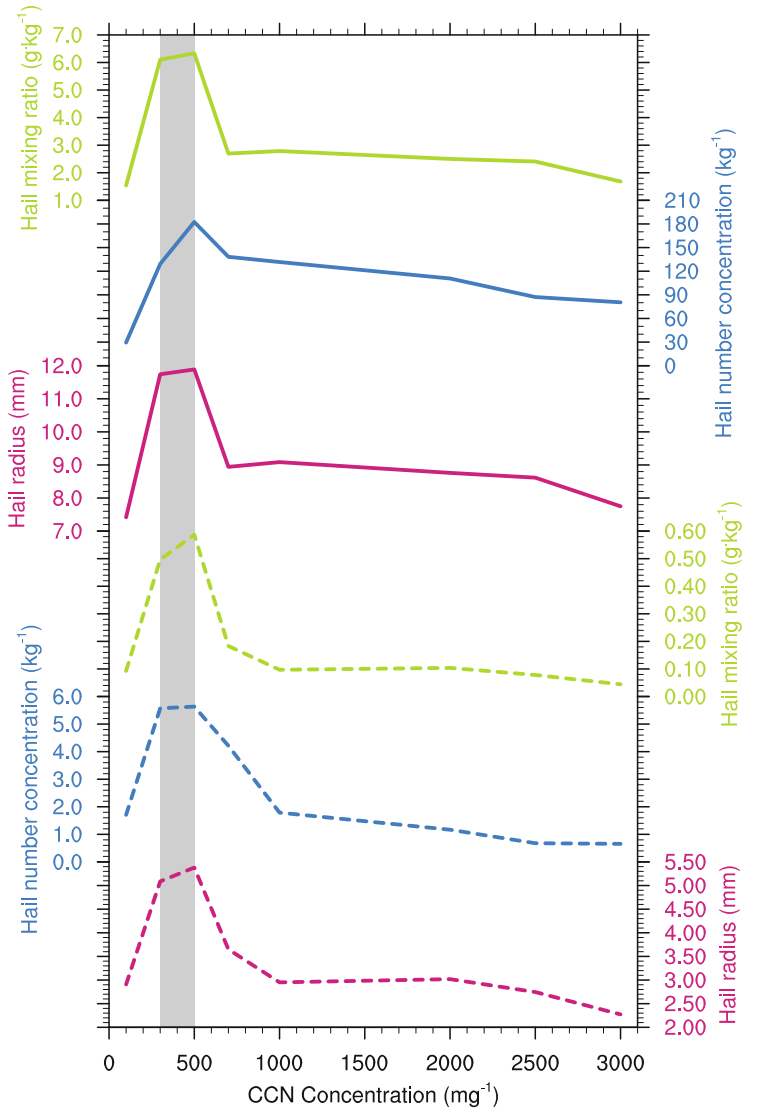

Fig. 4. Hail domain-maximum mixing ratio (green lines), maximum number concentration (blue lines), and maximum mean radius of hail size distribution (red lines), in clouds (solid lines) and at the surface (dashed lines), with respect to the initial CCNC. The shaded area is the CCNC threshold.

To investigate the microphysics latent heating effect on updraft volume, a vertical profile of the condensation and frozen latent heating among cases in Table 1 from 10–30 min and 35–55 min are shown in Figs. 6b and c, because greater updraft volumes are driven by increased microphysics latent heating (Mansell and Ziegler, 2013). There was a crucial mixed-phase region in the mature stage of hail formation between 4 and 8 km, where the mixing ratio and the number concentration of hail were highest (Fig. 3). In this region, the variable latent heating and variable updraft volume together determined the non-monotonic behavior of hail at different initial CCNCs. From 10–30 min between 4 and 8 km, peak values of the condensation latent heating rate increased from CCN100 to CCN3000, but there was nearly no difference above the CCNC threshold (CCN700, CCN1000 and CCN3000). However, the peak values of frozen latent heating for the cases below the CCNC threshold were concentrated between 4 and 8 km, while the cases above the CCNC threshold were concentrated between 8 and 10 km because of the formation of ice-phase hydrometeors at the higher level. That means the difference in frozen latent heating would greatly assist in increasing the updraft volume for cases below the CCNC threshold. Meanwhile, both the peak height of condensation and frozen latent heating increased from CCN100 to CCN3000. When the storm developed between 35 and 55 min, all the peak values of condensation latent heating showed a close pattern of around 0.12 K s^{-1} between 4 and 6 km, except CCN100, while the frozen latent heating in cases below the CCNC threshold were still greater than above the CCNC threshold near 6 km in height. The peak frozen latent heating values of CCN300 and CCN500 were greater than 0.05 K s^{-1} near 6 km in height. When the CCNC was be-

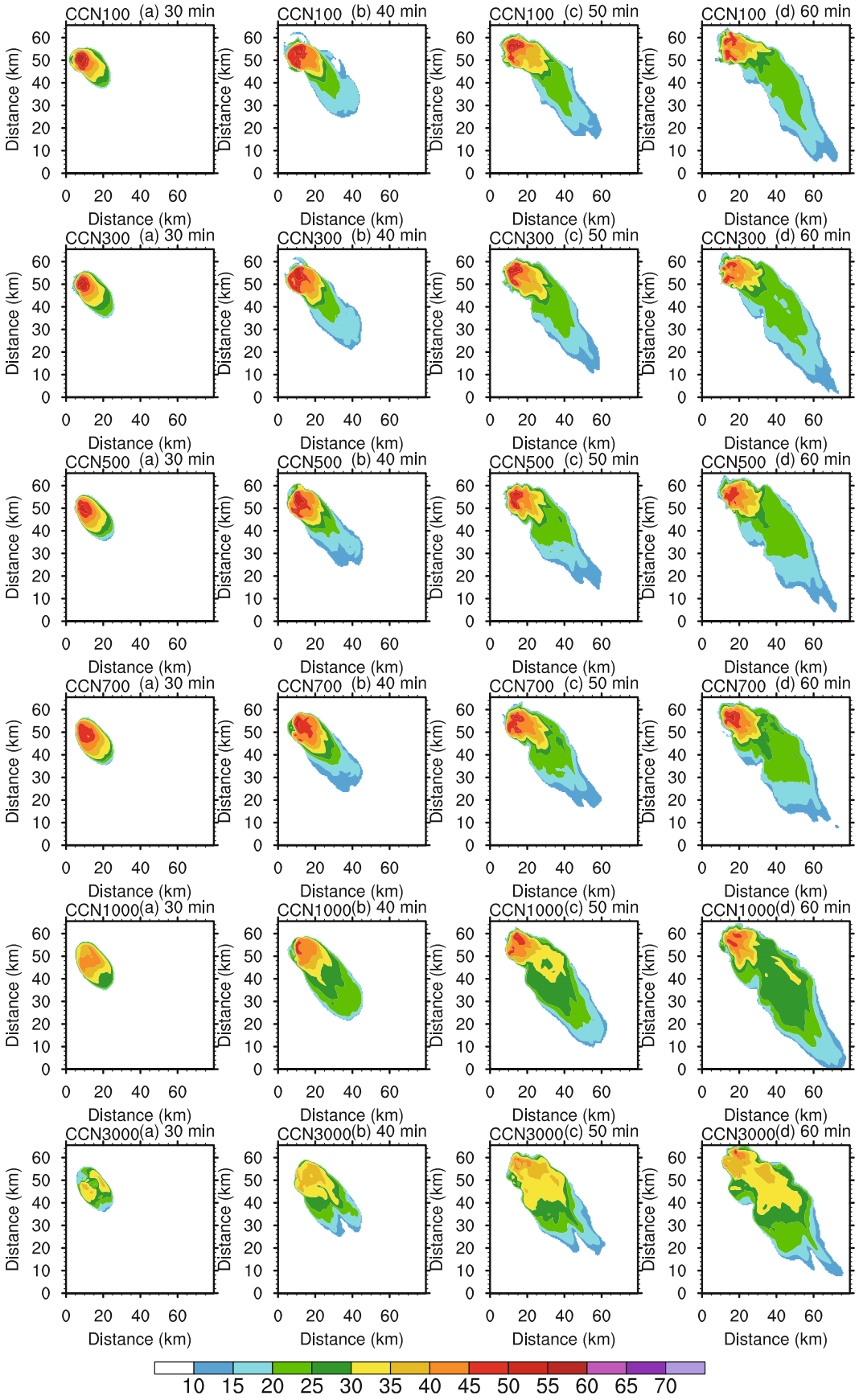

Fig. 5. Simulated domain-maximum equivalent radar composite reflectivity factor, in dBZ, with simulation times from 30 min to 60 min [Column (a): 30 min; Column (b): 40 min; Column (c): 50 min; Column (d): 60 min], for the cases in Table 1.

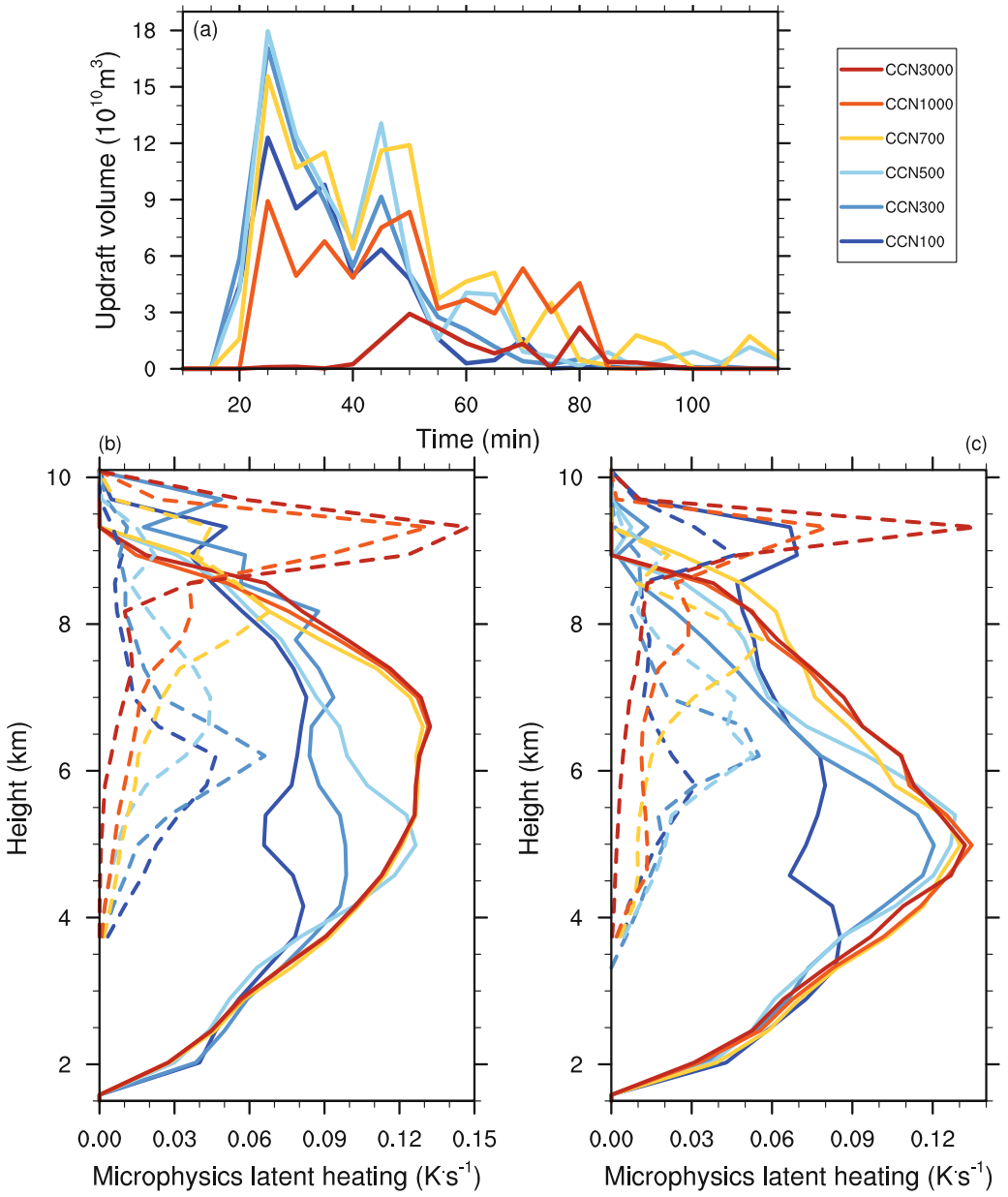

Fig. 6. (a) Time series of updraft volume (updraft speed greater than 10 m s^{-1}; radar reflectivity greater than 35 dBZ; temperature below 0°C), in 10^{10} m^3, for the cases in Table 1. (b, c) Domain-maximum latent heating profiles of vapor condensation (solid lines) and liquid water frozen (dashed lines), in K s^{-1}, from (b) 10–30 min and (c) 35–55 min, for the cases in Table 1.

low the CCNC threshold, the increased CCNC resulted in more cloud water and more liquid water being frozen into ice-phase hydrometeors between 4 and 8 km, which released a greater amount of latent heat from vapor condensation and liquid water frozen causing a stronger updraft volume (Fig. 6a). When the CCNC was above the CCNC threshold, the increased CCNC could only lead to a little more condensation latent heating between 6 and 8 km with more and smaller cloud water droplets, which were quickly lifted to higher altitudes to form ice-phase hydrometeors, so that the center region of frozen latent heating was higher between 8 and 10 km, causing a decrease in updraft volume. Furthermore, it led to the reduced rain auto-conversion process and reduced parcel buoyancy that could be attributed to a combination of increased mass loading by cloud droplets (Mansell and Ziegler, 2013), and the steady reduction in rain production would in turn result in less freezing because there were fewer and fewer frozen rain drops to act as embryos for rapidly growing graupel. Therefore, the thermodynamic effects cannot be isolated from the microphysics effects.

3.4. *Microphysical effects of CCN*

Hail formation and growth rely not only on the dynamical but also the microphysical effects of CCN on all other

hydrometeor fields. The four dominant hail-increasing processes were as follows: collection of rain water by hail, collection of cloud droplets by hail, conversion of graupel to hail, and collection of snow by hail. The three dominant hail-decreasing processes and their percentage contributions in all six cases were as follows: melting of hail to rain, shedding of hail to rain, and sublimation of hail (Fig. 7).

The increased CCNC in cases CCN100–CCN3000 led to obvious increases in the total mass but decreases in the mean radius of cloud droplets (Fig. 8). The simulations assumed that a higher CCNC would result in higher cloud water content in the early stage of cloud evolution. There was also a delay in the formation of rain drops, resulting primarily from the slowed auto-conversion rate of small cloud droplets into rain drops, resulting in a decrease in the total mass of rain drops and reduced mass loading. The increase in the radius of rain drops under higher CCNCs might be caused by the melting of large ice-phase hydrometeors (Fig. 8). As the CCNC increased below the CCNC threshold, the net riming rate increased drastically between 4 and 8 km at 30 min. As the CCN increased above the CCNC threshold, the rain auto-conversion process was effectively reduced and the net riming rate decreased between 4 and 8 km, and its appearance was delayed to 40 min (Fig. 9). The results show that the riming rate was very consistent with the mixing ratio of hail (Fig. 3). The riming process of hail consists of the collection of cloud droplets and rain water. Below the CCNC threshold, the collection of rain water had a crucial role in the riming process due to the increased rain water radius, whereas above the CCNC threshold the collection of cloud droplets and rain water were both important in the riming process, due to the reduced mixing ratio of rain water (Figs. 8 and 9). Although the riming rate reached a maximum in case CCN500, the hail-decreasing process also reached a maximum in case CCN500. The net increase in the rate of hail formation reached a maximum in case CCN300, which was within the CCNC threshold domain (Fig. 7).

The increase in the CCNC also had an influence on the total mass and equivalent sphere radius of ice-phase hydrometeors. Large increases in the ice crystal total mass and a decrease in the equivalent sphere radius in cases CCN100 to CCN3000 can be seen in Fig. 8. The increase in the CCNC caused a continual increase in the cloud total mass, but resulted in a decrease in the average cloud droplet radius. Thus, as the CCNC increased to the CCNC threshold, a mass of small cloud droplets was transported above the freezing level, enhancing heterogeneous nucleation and homogeneous nucleation processes, resulting in a larger number of smaller-sized ice crystals. As the CCNC increased above the CCNC threshold, a larger mass of smaller cloud droplets was transported to a higher altitude to form an even greater number of ice crystals, even smaller in size. The increased growth of ice crystals through vapor deposition led to an increase in the conversion of ice to snow. Snow aggregation was also enhanced. Therefore, increases in both the total mass and radius of snow were also apparent as the CCNC increased, resulting in a continued growth in the collection of snow by hail (Fig. 7).

In all cases, graupel formed after approximately 20 min of simulation time, as can be seen from the time series of the total mass of graupel (Fig. 8). The response of graupel to the CCNC was similar to that of hail. The increase in the CCNC from case CCN100 to CCN700 led to an increase in the total mass of graupel, as more cloud water droplets were frozen into the graupel in the enhanced net riming process, and more ice and snow were converted to graupel embryos at high levels. This is consistent with Mansell and Ziegler (2013) in that most graupel was produced by rain drop freezing until the CCNC threshold; although, the peak CCNC was lower than theirs, possibly due to the weaker convection environment. However, the increase in the CCNC from cases CCN700 to CCN3000 led to a decrease in the mixing ratio of graupel, due to the reduced initiation of graupel by the riming process of smaller ice crystals at high levels. Therefore, a minimum rime density and fewer large supercooled rain droplets were available to be frozen into graupel in the model (Fig. 9). Consequently, the average conversion rate of graupel to hail increased from case CCN100 to CCN300, and then decreased to case CCN3000 (Fig. 7).

There was a delay in the formation of hail from 20 min to 40 min (Fig. 8), which was not the case for graupel, where there was no delay from cases CCN100 to CCN3000, because of the different initiations of hail and graupel embryos. Graupel was initiated by the riming of ice crystals or snow particles, which were abundant in all CCN conditions with a sufficient riming rate and riming density. But, hail embryos were initiated by the conversion of large graupel whose growth was limited by the riming process of smaller ice crystals, and snow particles at high levels in different CCN conditions. Below the CCNC threshold, the mixing ratio and the number concentrations of hail increased from cases CCN100 to CCN500, mainly due to the enhanced riming process and the enhanced conversion of graupel to hail, with the ease of wet growth due to the riming conditions. Above the CCNC threshold, the increase in the CCNC from case CCN700 to CCN3000 led to a decrease in the mixing ratio and number concentration of hail. As the radius of cloud droplets decreased, it led a decrease in the collection of cloud droplets and auto-conversion by raindrops, so that less rain water was available to support the collection of itself by hail (Figs. 7 and 8). Meanwhile, smaller cloud droplets reduced the riming density on ice-phase hydrometeors, so that graupel density was lower and less graupel was then available to sustain the wet growth condition and enable conversion into hail in the core region of the storm.

4. Conclusions and discussion

In this study, the effects of the initial CCNC on hail properties from the perspectives of thermodynamics and microphysics were evaluated using the WRF model with the NSSL 2-moment bulk scheme in a 3D idealized hail storm simulation with a non-severe but typical sounding in China. The results demonstrate that an increase in CCNC from 100 to

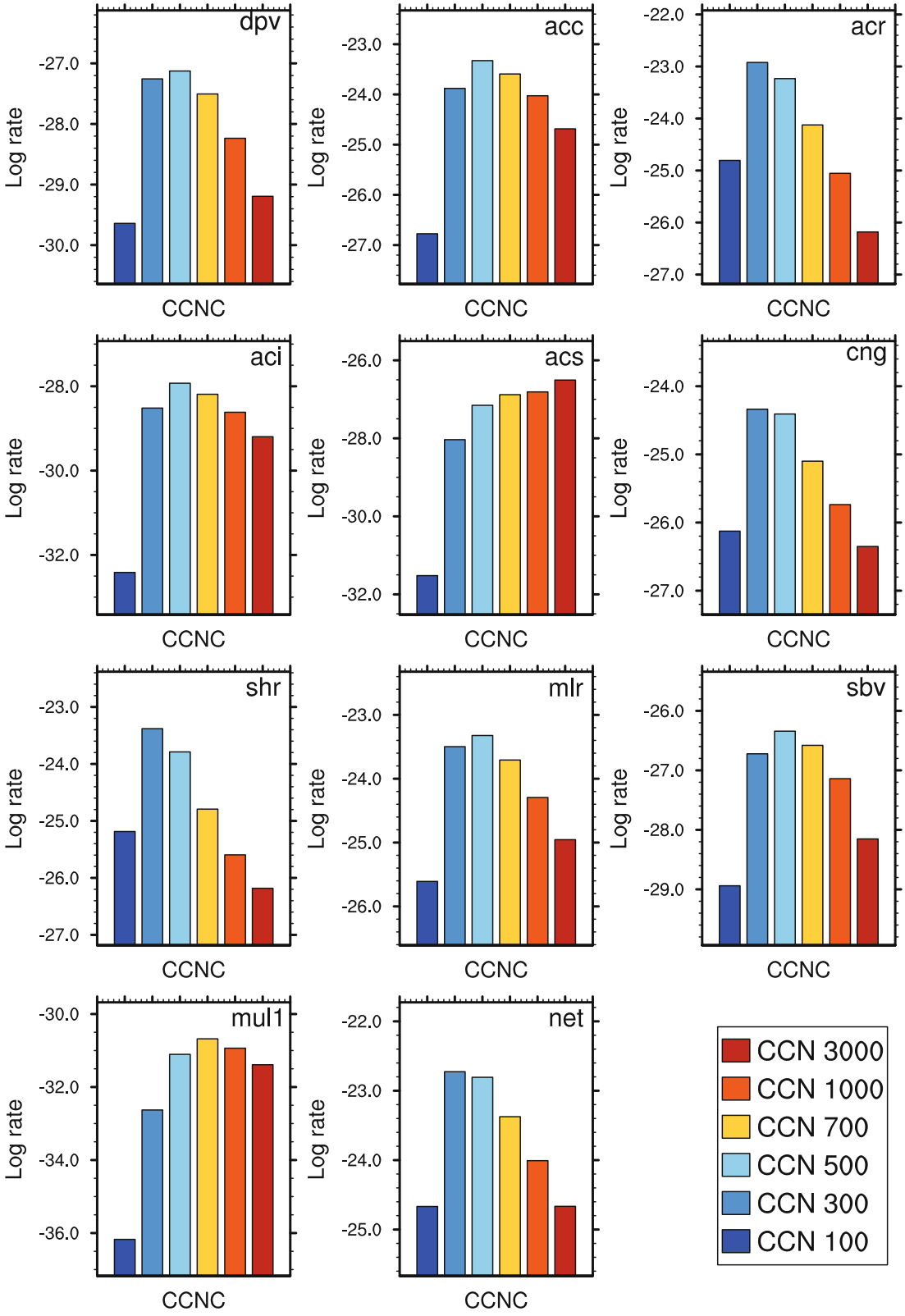

Fig. 7. Bar charts showing the average rate of the individual processes in the overall hail-increasing process, hail-decreasing process, and net increase, in kg kg^{-1} s^{-1}, on the logarithmic scale, for the six cases in Table 1. The hail-increasing process contains the following individual processes: deposition of vapor to hail (dpv), collection of cloud droplets by hail (acc), collection of rain water by hail (acr), collection of ice crystals by hail (aci), collection of snow by hail (acs), and conversion of graupel to hail (cng). The hail-decreasing process contains the following individual processes: sublimation of hail (sbv), shedding of hail to rain (shr), melting of hail to rain (mlr), and multiplication of ice (mul1).

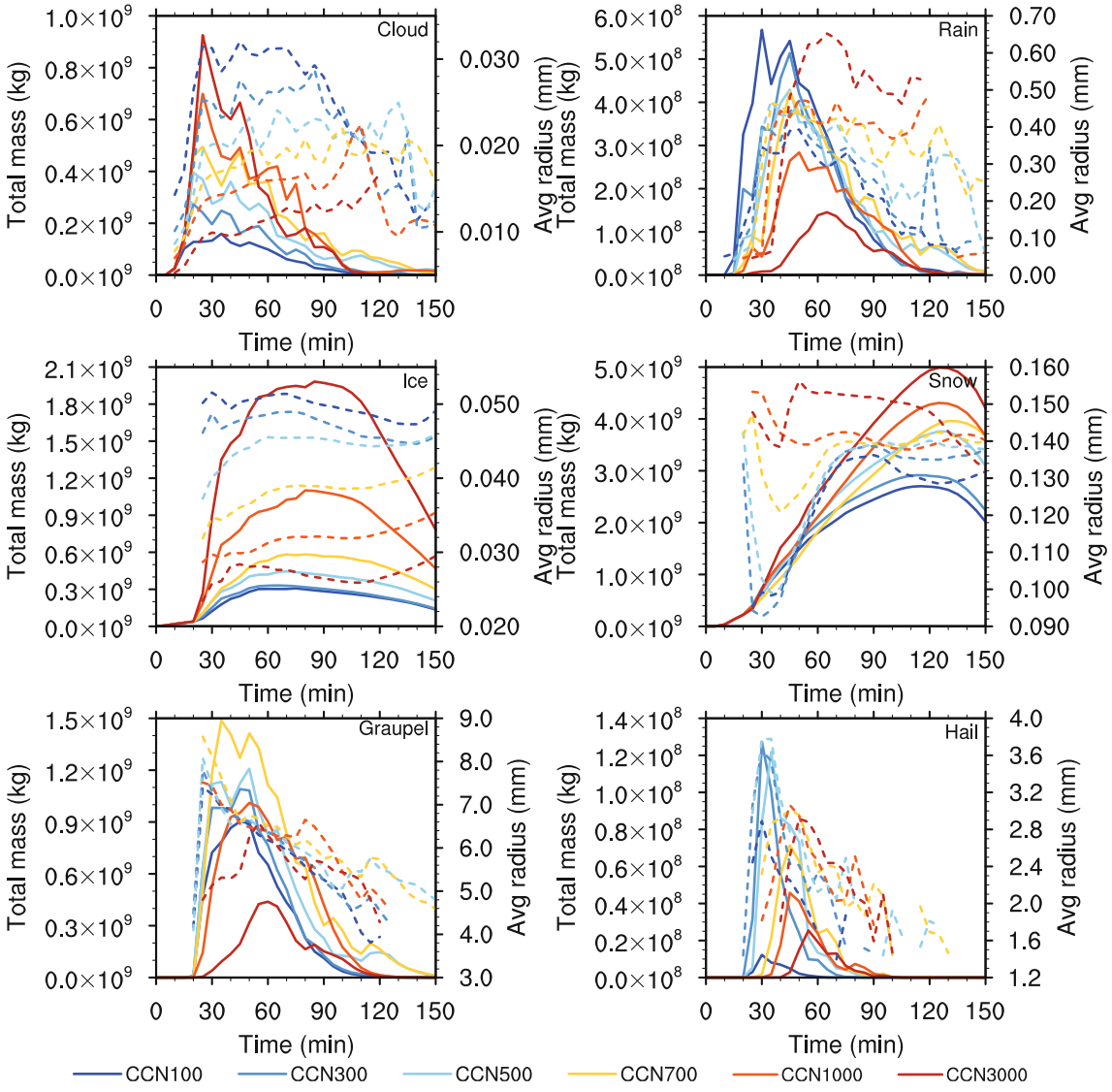

Fig. 8. Time series of the total mass, in kg (solid lines), and equivalent sphere radius, in mm, (dashed lines), for the six types of hydrometeors for the cases in Table 1.

3000 mg^{-1} has an impact on hail properties, including the mass mixing ratio, number concentration, and mean radius of hailstones. Increased CCN leads to more small cloud water droplets, which are lifted to high levels to form more small ice crystals and snow. This leads to a decrease in the initiation of hail, meaning delays occur in the formation of hail and in the maximum radar composite reflectivity, as well as in the surface hail precipitation, with the increasing initial CCNC.

The initial CCNC has an evident non-monotonic impact on hail, with a CCNC threshold value between 300 and 500 mg^{-1}, both in clouds and at the surface.

The following is a summary of the key findings regarding the mechanisms:

(1) Below the CCNC threshold value, the mixing ratio and number concentration of the small particles (i.e., cloud droplets and ice crystals) is positively correlated with the CCNC in the abundant water vapor environment in clouds. Consequently, more condensation latent heat is released and the center region of frozen latent heating is concentrated between 4 and 8 km altitude in the mature stage of the storm, causing stronger updraft volume. More liquid cloud water and rain drops are then carried to higher altitudes to be collected by the graupel and hail embryos; therefore, surface hail precipitation is enhanced.

(2) Above the CCNC threshold value, continued increases in the CCNC lead to a huge number of smaller cloud droplets sharing the relatively limited amount of water vapor in clouds, resulting in a reduction in the warm-rain process. Therefore, more cloud droplets are lifted to the higher frozen altitude, leaving too few supercooled rain drops in the mixed-phase region. The lack of supercooled rain drops leads to less frozen drop production and therefore suppresses the riming process of small graupel and hail particles, so the mixing ratio, number concentration and maximum mean radius of the hail size distribution decrease in clouds, and surface hail precipitation is reduced.

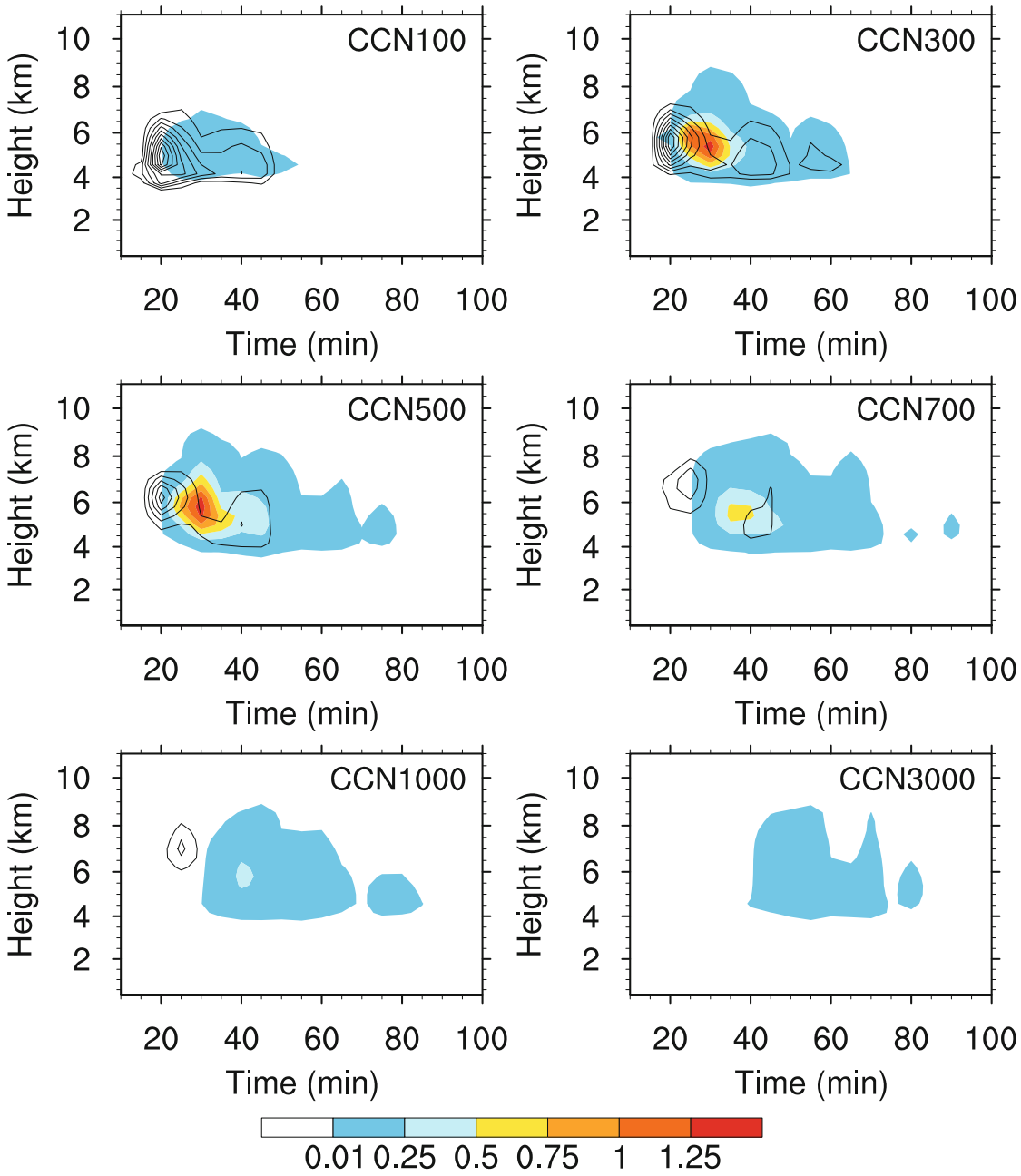

Fig. 9. Time–height contours of the domain-averaged net hail riming rate, in mg kg^{-1} s^{-1} (color fill), and the mixing ratio of supercooled rain water, in g kg^{-1} (black contours from 0 to 1.5 by 0.15), for the cases in Table 1. The net riming rate is calculated by acc + acr − shr (in Fig. 7), and supercooled rain water is defined as the rain water where air temperature is below 0°C.

In addition, the surface hail precipitation rate seems to be positively associated with the maximum peak value of updraft volume and microphysics latent heating between 4 and 8 km in the mature stage of the storm. Regarding the surface total precipitation rate, an increased CCNC leads to a reduction in the warm-rain process; smaller rain drops require more time to collect smaller cloud droplets, resulting in a delay in the formation of larger rain drops. The terminal fall speed of small ice crystals and snow at high altitudes is reduced with an increase in the initial CCNC, resulting in a reduced density and fall speed of graupel, and further contributing to the delayed surface total precipitation and extending the cloud anvil area. Moreover, the total precipitation rate responds monotonically to an increase in the CCNC. More CCN have a suppressive effect on the total precipitation rate and an inhibitory effect on the intensity of the hail storm when the CCNC is well above the CCNC threshold because of the reduced parcel buoyancy and mass loading (Mansell and Ziegler, 2013).

This study was based on a hail storm simulation with a 2-moment bulk microphysical scheme, and it predicted the

mixing ratio and number concentration for six hydrometeor species. The input sounding was based on a monsoon-area case in summer in China, where the environmental conditions (e.g., moisture layer, CAPE, and wind shear) differed from those in previous studies [although Carrió et al. (2014) investigated the increased sensitivity of hail to CCN with increasing cloud-base height]. Whether the above-mentioned factors are the determining factors of the CCN impact on hail should be investigated further. Our input sounding data had several similarities and differences with those of Loftus and Cotton (2014) and Mansell and Ziegler (2013). For example, we had almost the same lifting condensation level and temperature at the lifting level. However, our CAPE value and wind shear were lower than theirs, and our water vapor value was higher. The observation and simulation of hail size up to about 6 mm and the weaker input sounding would put this case in a non-severe category, which may have had hail particles forming within a simpler updraft rather than recycling in a severe hailstorm. The current study was based on a relatively short-term investigation that ignored the dynamic and thermodynamic feedbacks between the hail storm system and its large-scale environment. Moreover, the occurrences of hail in China are always different between the eastern and western parts, where the base soundings of the storms are also always different (Li et al., 2016; Wang et al., 2016a). Therefore, it remains to be determined whether the effect of the CCNC on hail varies with different input soundings, and longer-time-scale hail storm responses to CCN should also be investigated.

Acknowledgements. This study was supported by the National Natural Science Foundation of China (Grant Nos. 41330421 and 41461164006) and the Chinese 973 program (Grant No. 2013CB430104). The authors also acknowledge the editor and anonymous reviewers, whose valuable comments and suggestions significantly improved this article.

REFERENCES

Andreae, M. O., and D. Rosenfeld, 2008: Aerosol–cloud–precipitation interactions. Part 1. The nature and sources of cloud-active aerosols. *Earth-Science Reviews*, **89**, 13–41, doi: 10.1016/j.earscirev.2008.03.001.

Carrió, G. G., W. R. Cotton, and A. M. Loftus, 2014: On the response of hailstorms to enhanced CCN concentrations. *Atmos. Res.*, **143**, 342–350, doi: 10.1016/j.atmosres.2014.03.002.

Cotton, W. R., G. J. Tripoli, R. M. Rauber, and E. A. Mulvihill, 1986: Numerical simulation of the effects of varying ice crystal nucleation rates and aggregation processes on orographic snowfall. *J. Climate Appl. Meteor.*, **25**, 1658–1680, doi: 10.1175/1520-0450(1986)025<1658:NSOTEO>2.0.CO;2.

Deierling, W., and W. A. Petersen, 2008: Total lightning activity as an indicator of updraft characteristics. *J. Geophys. Res.*, **113**, D16210, doi: 10.1029/2007JD009598.

Duan, J., Y. Chen, and X. L. Guo, 2012: Characteristics of aerosol activation efficiency and aerosol and CCN vertical distributions in North China. *Acta Meteorologica Sinica*, **26**(5), 579–596, doi: 10.1007/s13351-012-0504-6.

Fan, J., L. R. Leung, D. Rosenfeld, Q. Chen, Z. Li, J. Zhang, and H. Yane, 2013: Microphysical effects determine macrophysical response for aerosol impacts on deep convective clouds. *P. Natl. Acad. Sci. USA*, **110**, E4581–E4590, doi: 10.1073/pnas.1316830110.

Grabowski, W. W., 2014: Extracting microphysical impacts in large-eddy simulations of shallow convection. *J. Atmos. Sci.*, **71**, 4493–4499, doi: 10.1175/JAS-D-14-0231.1.

Grabowski, W. W., 2015: Untangling microphysical impacts on deep convection applying a novel modeling methodology. *J. Atmos. Sci.*, **72**, 2446–2464, doi: 10.1175/JAS-D-14-0307.1.

Guo, X. L., D. H. Fu, X. Y. Li, Z. X. Hu, H. C. Lei, H. Xiao, and Y. C. Hong, 2015: Advances in cloud physics and weather modification in China. *Adv. Atmos. Sci.*, **32**(2), 230–249, doi: 10.1007/s00376-014-0006-9.

Jia, X. P., G. Xin, Y. Qian, and Y. Qian, 2016: Sectoral co-control of air pollutants: Case of a chlor-alkali/polyvinyl chloride sector in China. *Journal of Cleaner Production*, **112**, 1667–1675, doi: 10.1016/j.jclepro.2015.01.074.

Jiang, H. Y., 2012: The relationship between tropical cyclone intensity change and the strength of inner-core convection. *Mon. Wea. Rev.*, **140**(4), 1164–1176, doi: 10.1175/MWR-D-11-00134.1.

Jiang, J., D. P. Jiang, and Y. H. Lin, 2015: Monsoon area and precipitation over China for 1961–2009. *Chinese Journal of Atmospheric Sciences*, **39**, 722–730, doi: 10.3878/j.issn.1006-9895.1410.14195. (in Chinese)

Khain, A., D. Rosenfeld, and A. Pokrovsky, 2005: Aerosol impact on the dynamics and microphysics of deep convective clouds. *Quart. J. Roy. Meteor. Soc.*, **131**, 2639–2663, doi: 10.1256/qj.04.62.

Khain, A., D. Rosenfeld, A. Pokrovsky, U. Blahak, and A. Ryzhkov, 2011: The role of CCN in precipitation and hail in a mid-latitude storm as seen in simulations using a spectral (bin) microphysics model in a 2D dynamic frame. *Atmos. Res.,* **99**, 129–146, doi: 10.1016/j.atmosres.2010.09.015.

Li, M. X., Q. H. Zhang, and F. Q. Zhang, 2016: Hail day frequency trends and associated atmospheric circulation patterns over China during 1960–2012. *J. Climate.*, **29**, 7027–7044, doi: 10.1175/JCLI-D-15-0500.1.

Li, G. H., Y. Wang, and R. Y. Zhang, 2008: Implementation of a two-moment bulk microphysics scheme to the WRF model to investigate aerosol-cloud interaction. *J. Geophys. Res.*, **113**, D15211, doi: 10.1029/2007JD009361.

Liu, X. L., and S. J. Niu, 2010: Numerical simulation of macro- and micro-structures of intense convective clouds with a spectral bin microphysics model. *Adv. Atmos. Sci.*, **27**(5), 1078–1088, doi: 10.1007/s00376-010-8088-5.

Loftus, A. M., and W. R. Cotton, 2014: Examination of CCN impacts on hail in a simulated supercell storm with triple-moment hail bulk microphysics. *Atmos. Res.*, **147–148**, 183–204, doi: 10.1016/j.atmosres.2014.04.017.

Mansell, E. R., 2010: On sedimentation and advection in multimoment bulk microphysics. *J. Atmos. Sci.*, **67**, 3084–3094, doi: 10.1175/2010JAS3341.1.

Mansell, E. R., and C. L. Ziegler, 2013: Aerosol effects on simulated storm electrification and precipitation in a two-moment bulk microphysics model. *J. Atmos. Sci.*, **70**, 2032–2050, doi: 10.1175/JAS-D-12-0264.1.

Mansell, E. R., C. L. Ziegler, and E. C. Bruning, 2010: Simulated electrification of a small thunderstorm with two-

moment bulk microphysics. *J. Atmos. Sci.*, **67**, 171–194, doi: 10.1175/2009JAS2965.1.

Noppel, H., U. Blahal, A. Seifert, and K. D. Beheng, 2010: Simulations of a hailstorm and the impact of CCN using an advanced two-moment cloud microphysical scheme. *Atmos. Res.*, **96**, 286–301, doi: 10.1016/j.atmosres.2009.09.008.

Phillips, V. T. J., P. J. DeMott, and C. Andronache, 2008: An empirical parameterization of heterogeneous ice nucleation for multiple chemical species of aerosol. *J. Atmos. Sci.*, **65**, 2757–2783, doi: 10.1175/2007JAS2546.1.

Rosenfeld, D., 2000: Suppression of rain and snow by urban and industrial air pollution. *Science*, **287**, 1793–1796, doi: 10.1126/science.287.5459.1793.

Rosenfeld, D., U. Lohmann, G. B. Raga, C. D. O'Dowd, M. Kulmala, S. Fuzzi, A. Reissell, and M. O. Andreae, 2008: Flood or drought: how do aerosols affect precipitation? *Science*, **321**, 1309–1313, doi: 10.1126/science.1160606.

Seifert, A., A. Khain, A. Pokrovsky, and K. D. Beheng, 2006: A comparison of spectral bin and two-moment bulk mixed-phase cloud microphysics. *Atmos. Res.*, **80**, 46–66, doi: 10.1016/j.atmosres.2005.06.009.

Straka, J. M., 2009: *Cloud and Precipitation Microphysics: Principles and Parameterizations*. Cambridge University Press, 407 pp.

Sun, J. M., and P. A. Ariya, 2006: Atmospheric organic and bioaerosols as cloud condensation nuclei (CCN): A review. *Atmos. Environ.*, **40**, 795–820, doi: 10.1016/j.atmosenv.2005.05.052.

Sun, X., Y. Yin, Y. Han, H. Xiao, Y.-W. Sun, and B.-D. Li, 2012: Distribution characteristics of cloud particles and cloud condensation nuclei during haze/fog events in Shijiazhuang. *China Environmental Science*, **32**(7), 1165–1170. (in Chinese)

Szoke, E. J., and E. J. Zipser, 1986: A radar study of convective cells in mesoscale systems in GATE. Part II: Life cycles of convective cells. *J. Atmos. Sci.*, **43**, 199–218, doi: 10.1175/1520-0469(1986)043<0199:ARSOCC>2.0.CO;2.

Tao, W.-K., X. W. Li, A. Khain, T. Matsui, S. Lang, and J. Simpson, 2007: Role of atmospheric aerosol concentration on deep convective precipitation: cloud-resolving model simulations. *J. Geophys. Res.*, **112**, D24S18, doi: 10.1029/2007JD008728.

van den Heever, S. C., G. G. Carrió, W. R. Cotton, P. J. Demott, and A. J. Prenni, 2006: Impacts of nucleating aerosol on Florida storms. Part I: Mesoscale simulations. *J. Atmos. Sci.*, **63**, 1752–1775, doi: 10.1175/JAS3713.1.

van den Heever, S. C., G. L. Stephens, and N. B. Wood, 2011: Aerosol indirect effects on tropical convection characteristics under conditions of radiative–convective equilibrium. *J. Atmos. Sci.*, **68**, 699–718, doi: 10.1175/2010JAS3603.1.

Wang, J. A., Y. J. Yue, J. T. Zhao, Y. Bai, L. L. Lv, P. J. Shi, and W. J. Dong, 2016a: Snow, frost, and hail disasters in China. *Natural Disasters in China*, P. J. Shi, Ed., Springer, 187–237, doi: 10.1007/978-3-662-50270-9_7.

Wang, W., and Coauthors, 2016b: Weather Research & Forecasting ARW Version 3 Modeling System User's Guide. [Availiable on line at http://www2.mmm.ucar.edu/wrf/users/docs/user_guide_V3/ARWUsersGuideV3.pdf]

Xiao, H., H. Y. Xu, and M. Y. Huang, 1988: The study of numerical simulation on the formation of the cloud droplet spectra in cumulus Clouds—Part I: The roles of the spectra and concentrations of salt nuclei. *Scientia Atmospherica Sinica*, **12**(2), 121–130, doi: 10.3878/j.issn.1006-9895.1988.02.02. (in Chinese)

Xie, B. G., Q. H. Zhang, and Y. Q. Wang, 2010: Observed characteristics of hail size in four regions in China during 1980–2005. *J. Climate*, **23**, 4973–4982, doi: 10.1175/2010JCLI3600.1.

Yang, H.-L., H. Xiao, and Y.-C. Hong, 2011: A numerical study of aerosol effects on cloud microphysical processes of hailstorm clouds. *Atmos. Res.*, **102**, 432–443, doi: 10.1016/j.atmosres.2011.09.007.

Yin, Y., Z. Levin, T. G. Reisin, and S. Tzivion, 2000: The effects of giant cloud condensation nuclei on the development of precipitation in convective clouds—A numerical study. *Atmospheric Research*, **53**, 91–116, doi: 10.1016/S0169-8095(99)00046-0.

Ziegler, C. L., 1985: Retrieval of thermal and microphysical variables in observed convective storms. Part 1: Model development and preliminary testing. *J. Atmos. Sci.*, **42**, 1487–1509, doi: 10.1175/1520-0469(1985)042<1487:ROTAMV>2.0.CO;2.

Zhang, Q. H., X. Ni, and F. Q. Zhang, 2017: Decreasing trend in severe weather occurrence over China during the past 50 years. *Sci. Rep.*, **7**, 42310, doi: 10.1038/srep42310.